Stem Cell Reports
Report
OPEN ACCESS

Wilms' Tumor Blastemal Stem Cells Dedifferentiate to Propagate the Tumor Bulk

Rachel Shukrun,[1,2,7,8] Naomi Pode-Shakked,[1,2,3,7,8] Oren Pleniceanu,[1,2,7] Dorit Omer,[1,2,7] Einav Vax,[1,2,7] Eyal Peer,[2,7] Sara Pri-Chen,[4] Jasmine Jacob,[2] Qianghua Hu,[6] Orit Harari-Steinberg,[1,2] Vicki Huff,[6] and Benjamin Dekel[1,2,4,5,7,*]

[1]Pediatric Stem Cell Research Institute, Sheba Medical Center, Tel Hashomer 5262000, Israel
[2]Sheba Centers for Regenerative Medicine and Cancer Research, Sheba Medical Center, Ramat-Gan, Tel Hashomer 5262000, Israel
[3]Dr. Pinchas Borenstein Talpiot Medical Leadership Program 2013, Sheba Medical Center, Tel Hashomer 5262000, Israel
[4]The Maurice and Gabriela Goldschleger Eye Research Institute, Sheba Medical Center, Tel Hashomer 5262000, Israel
[5]Division of Pediatric Nephrology, Sheba Medical Center, Tel Hashomer 5262000, Israel
[6]Department of Genetics, MD Anderson Cancer Center, Houston, TX 77030, USA
[7]Sackler School of Medicine, Tel Aviv University, Tel Aviv 6997801, Israel
[8]Co-first author
*Correspondence: binyamin.dekel@sheba.health.gov
http://dx.doi.org/10.1016/j.stemcr.2014.05.013

SUMMARY

An open question remains in cancer stem cell (CSC) biology whether CSCs are by definition at the top of the differentiation hierarchy of the tumor. Wilms' tumor (WT), composed of blastema and differentiated renal elements resembling the nephrogenic zone of the developing kidney, is a valuable model for studying this question because early kidney differentiation is well characterized. WT neural cell adhesion molecule 1-positive ($NCAM1^+$) aldehyde dehydrogenase 1-positive ($ALDH1^+$) CSCs have been recently isolated and shown to harbor early renal progenitor traits. Herein, by generating pure blastema WT xenografts, composed solely of cells expressing the renal developmental markers SIX2 and NCAM1, we surprisingly show that sorted $ALDH1^+$ WT CSCs do not correspond to earliest renal stem cells. Rather, gene expression and proteomic comparative analyses disclose a cell type skewed more toward epithelial differentiation than the bulk of the blastema. Thus, WT CSCs are likely to dedifferentiate to propagate WT blastema.

INTRODUCTION

The cancer stem cell (CSC) model suggests that whereas most tumor cells are destined to differentiate, albeit aberrantly, a small subset of tumor cells, termed CSCs, actively sustain and propagate the tumor. Although CSCs are considered to be at the top of the differentiation hierarchy of the tumor, this has not been examined in human tumors. Wilms' tumor (WT), a prototype of differentiation failure in human cancer, shares the histology of the fetal kidney, including blastema, stroma, and differentiating tubular epithelium (Shukrun et al., 2014; Dekel et al., 2006; Pode-Shakked and Dekel, 2011; Rivera and Haber, 2005). Because normal renal differentiation is well characterized, WT represents an invaluable model for establishing the position of CSC with respect to this differentiation cascade.

Kidney development is initiated when the Wolffian duct sends off a dorsal branch, the ureteric bud (UB), to invade the metanephric mesenchyme (MM) (Pleniceanu et al., 2010). The UB receives MM-derived signals to undergo branching morphogenesis and develop into the collecting system. Reciprocally, a fraction of the MM, termed cap mesenchyme (CM), receives signals from the UB tips, facilitating its survival, proliferation, and mesenchymal-to-epithelial transition (MET) into nephron epithelia. Sequential steps during renal MET have been characterized by specific gene expression and signaling pathway activity. This process is accompanied by gradual loss of renal developmental factors and mesenchymal markers (e.g., SIX2, CITED1, and vimentin) and acquisition of epithelial proteins (e.g., E-Cadherin) (Cirio et al., 2014; Metsuyanim et al., 2009; Self et al., 2006). The CM has been recently shown to consist of true stem cells, capable of self-renewing and differentiating toward different types of nephron epithelia (Cirio et al., 2014; Kobayashi et al., 2008).

We have recently uncovered the identity of human WT CSCs. WT CSCs were isolated from trilineage WT (composed of blastema, stroma, and tubular epithelium) propagated in mice and characterized by high expression levels of neural cell adhesion molecule 1 (NCAM1) and aldehyde dehydrogenase 1 (ALDH1) enzymatic activity (Pode-Shakked et al., 2013). These cells possessed both self-renewal and multilineage differentiation capacities, in line with the CSC definition. Immunohistochemical (IHC) analysis of WTs revealed that the CSC population was exclusively localized and scattered within the NCAM1-expressing blastema (Pode-Shakked et al., 2013). The WT blastema, suggested to resemble the CM harboring multipotent embryonic renal stem cells, is classically regarded as a homogeneous unit. Thus, whereas our analysis demonstrated WT CSCs to overexpress the renal

developmental gene set (i.e., *SIX2*, *OSR1*, *PAX2*, and *SALL1*), compatible with early renal progenitor cells, it was confounded by the presence of mature elements, and the precise developmental phenotype in regard to renal lineage differentiation remained elusive.

Therefore, to pinpoint the exact stage of the WT CSC in respect to embryonic renal stem cell differentiation, high-resolution analysis of a pure blastema population is required. Here, we created an in vivo model of pure blastema WT via serial propagation of human WT xenograft (Xn). This allowed us to show that the WT blastema is a heterogeneous-differentiating cell population that follows the renal developmental MET axis. Within this differentiation gradient of WT blastema, we show that WT CSCs are committed epithelial progenitors, and not the earliest mesenchymal renal stem cells, the presumable WT cell of origin (Li et al., 2002). Hence, WT CSCs must possess both dedifferentiation capacity forming less-differentiated, SIX2-high blastemal cells, as well as epithelial differentiation capability, as previously shown for NCAM1$^+$ALDH1$^+$ WT CSCs (Pode-Shakked et al., 2013). Dedifferentiation of WT CSCs into early mesodermal cells might also explain the presence of heterologous mesodermal elements such as muscle and bone seen in some WTs (Royer-Pokora et al., 2010).

RESULTS

Generation of Pure Blastema WT Xns

Previous work in our lab demonstrated that whereas WT blastema is lost upon in vitro propagation, generation of WT Xn preserves and even expands the blastema in vivo (Dekel et al., 2006; Metsuyanim et al., 2009). Here, we show that late-generation (passages 10–15) Xns are composed solely of homogeneous-appearing sheets of blastema cells (Figure 1A). Recently, utilizing low-passage WT Xns (passages 1–5), which maintain most of the primary tumor's properties (i.e., gene expression and trilineage histology), we isolated CSCs that exclusively initiate and sustain the tumor in vivo (Dekel et al., 2008). These NCAM1$^+$ALDH1$^+$ WT CSCs were shown to harbor renal stem cell characteristics compared to all other tumor components (Pode-Shakked et al., 2013). To further analyze late-generation Xns, we examined NCAM1 expression in comparison with primary human WT and early WT Xns. IHC revealed NCAM1 enrichment along serial passages of the tumor in mice (Figures 1B and 1C, left panel). Flow cytometry analysis performed on late Xns demonstrated that 100% of the cells express NCAM1 (Figure S1A available online). In addition, IHC showed these pure blastema WT Xn cells to uniformly express SIX2. (Figure 1C, middle panel). Altogether, pure blastema WT Xns are solely composed of NCAM1$^+$SIX2$^+$ cells, indicating their primitive renal nature.

The Tumorigenic Potential of Pure Blastema WT Xns Is Maintained Solely by the ALDH1$^+$ Cell Population

Establishment of pure blastema Xns afforded the opportunity to sort single ALDH1$^+$ cells and determine whether they exclusively function as CSCs and investigate their lineage relationship to all other non-CSC blastema cells. Localization of ALDH1 was initially determined in the pure blastema model using IHC. Scattered ALDH1$^+$ cells were localized within the SIX2$^+$ blastema (Figure 1C, right panel; Figure S1B). Late Xn cells were then sorted according to ALDH1 activity with high efficiency as shown via quantitative real-time PCR analysis (Figure S2A). Limiting-dilution xenotransplantation experiments revealed that only ALDH1$^+$ cells have the capacity to form tumors. Moreover, as few as 200 cells were sufficient to form new WT Xns, demonstrating the high tumorigenic potential of ALDH1$^+$ cells (Figure 2A). Thus, as in early passages, in these late passages, the ability to sustain and propagate the tumor is maintained solely by ALDH1$^+$ cells. Because resistance to conventional radio- and chemotherapies is a trait of CSCs in several malignancies (Bonnet and Dick, 1997; Reya et al., 2001), we examined the in vitro response of ALDH1$^+$ WT cells to radiation. Following exposure of WT Xn cells to ionizing radiation, an increase in ALDH1$^+$ cells was noted (Figure 2B). Moreover, the percentage of ALDH1$^+$ cells correlated with exposure time and radiation intensity in a dose-dependent manner (Figure 2C). Hence, ALDH1$^+$ WT CSCs demonstrate increased resistance to conventional radiation treatment. Taken together, these results indicate that ALDH1$^+$ cells function as CSCs in pure blastema Xns.

Analysis of WT CSC Fraction in Relation with Embryonic Renal Differentiation Reveals Developmental Heterogeneity in WT Blastema

We have previously shown that early WT Xns derived from sorted NCAM1$^+$ALDH1$^+$ CSCs harbor a higher percentage of ALDH1$^+$ cells compared to tumors derived from unsorted cells (USs). In order to determine whether this trait is retained in pure blastema WT Xns, we compared ALDH1 expression between late Xns derived from ALDH1$^+$ sorted cells and those derived from USs. Fluorescence-activated cell sorting (FACS) analysis revealed that the former are enriched for ALDH1$^+$ CSCs (21.2% versus 5.6%, respectively) (Figures 3A, 3B, and S2B). Next, we performed global gene expression and proteomic analyses on these CSC-enriched (CSC-En) tumors in comparison with tumors derived from USs from the same tumor source (Figures 3C, 3D, and Table S1, respectively). We performed a microarray gene expression analysis comparing three samples: (1) human fetal

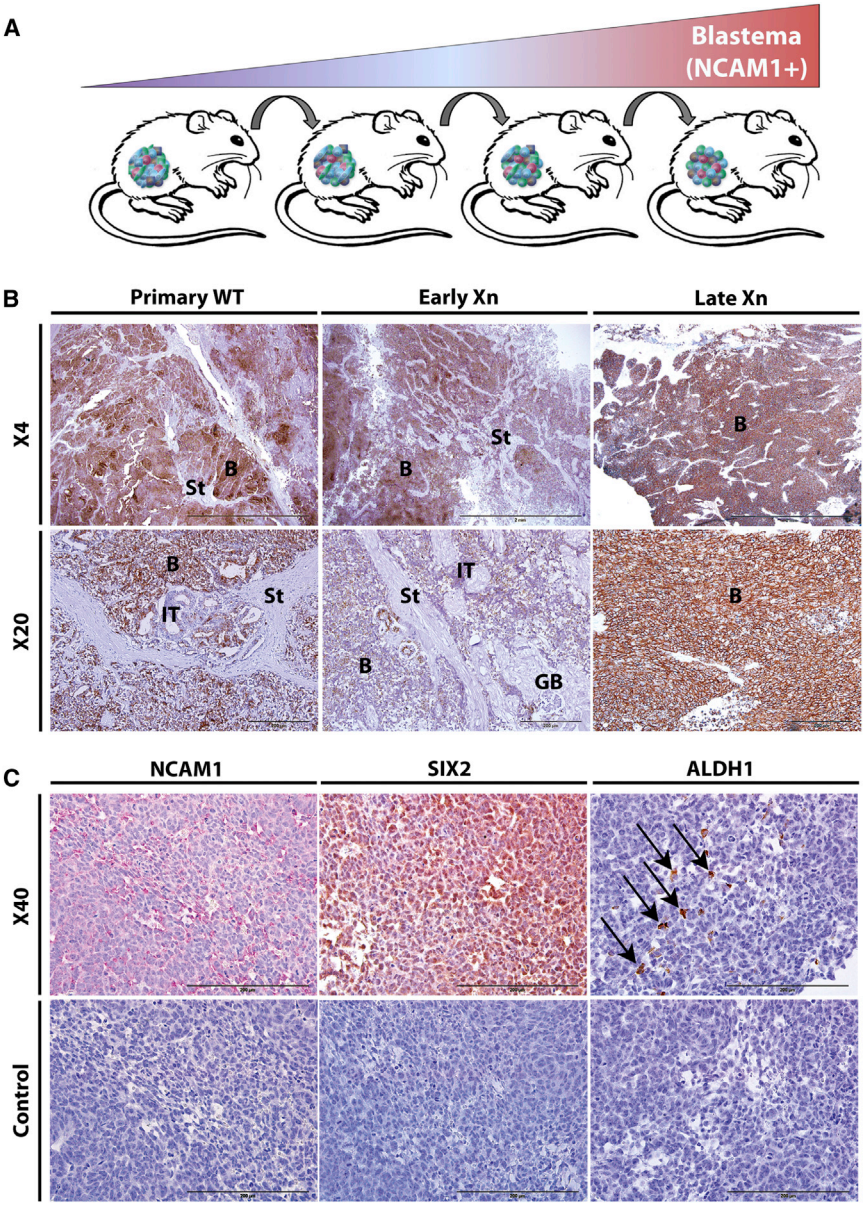

Figure 1. Generation of Pure Blastema WT Xns

(A) Serial propagation of human WT Xn in NOD-SCID mice results in enrichment of NCAM1$^+$ WT blastema, at the expense of differentiated structures.

(B) IHC staining of pWTs, early-passage Xns, and late-passage Xns for NCAM1. Early passages show great histological similarity to their parent tumor (B, blastema; IT, immature tubule; St, stroma; GB, glomeruloid bodies) with minor enrichment for the blastema (NCAM1$^+$) compartment. However, late-passage Xns are composed of 100% NCAM1$^+$ blastemal cells and are devoid of differentiated elements. Scale bars, 2 mm (top) and 200 μm (bottom).

(C) IHC staining of pure blastema WT Xns for NCAM1 (right), SIX2 (middle), and ALDH1 (left). All the tumor cells are NCAM1$^+$SIX2$^+$, whereas ALDH1$^+$ cells are scattered within these blastemal sheets. Scale bars, 200 μm. See also Figure S1.

kidney (hFK), (2) US tumors, and (3) CSC-En tumors. First, we performed hierarchical clustering in order to characterize the three samples with respect to the renal developmental signature, as manifested by the expression of several renal developmental genes (i.e., *SIX2*, *SALL1*, *OSR1*, *CITED1*, and *PAX2*). The results demonstrated genetic proximity between the two Xn samples, both expressing high levels of the aforementioned genes, compared to hFK, confirming that the pure blastema Xns harbor properties of primitive renal tissue. Interestingly, when comparing the two Xn samples, we found that CSC-En Xns expressed lower levels of the renal developmental genes (Figure 3C). We next carried out a quantitative real-time PCR analysis comparing the two Xn samples. This comparison validated the lower expression levels of the renal developmental gene set in the CSC-En sample. Importantly, CSC-En tumors showed higher expression of stemness genes (i.e., *NANOG*, *BMI1*, and *EZH2*), supporting enrichment for WT CSCs (Figure 3D). In addition, proteomic analysis supported the gene expression data, demonstrating a relative epithelial phenotype (i.e., high E-Cadherin) of the CSC-En tumors compared to US tumors (Table S1). Concomitantly, CSC-En tumors show upregulation of stemness-associated signaling pathways at the protein level (e.g., nuclear factor-κB [NF-κB], Wnt, phosphatidylinositol 3-kinase [PI3K], and mammalian target

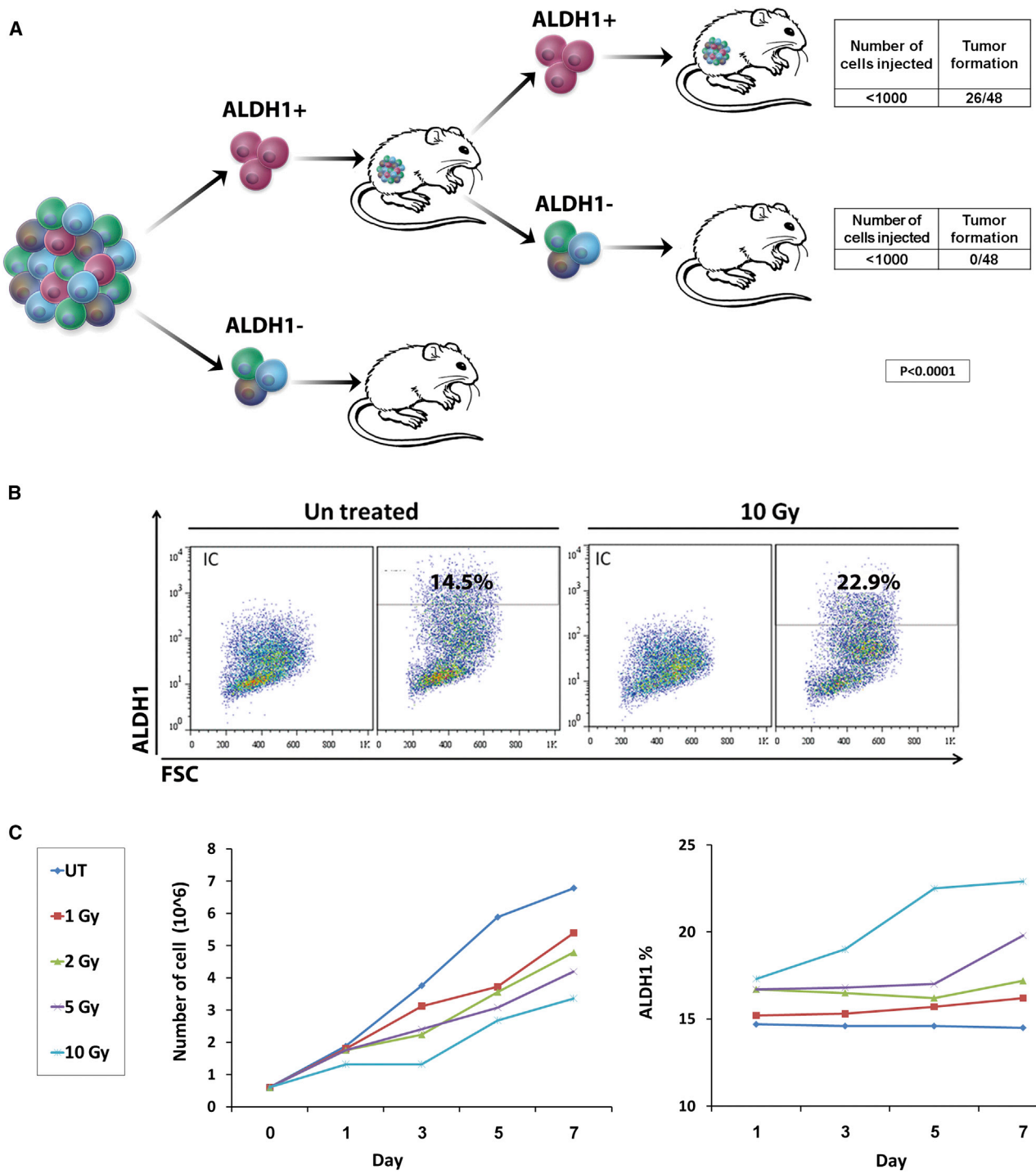

Figure 2. The Tumorigenic Potential of Pure Blastema WT Xns Is Maintained Solely by the ALDH1$^+$ Cell Population

(A) Scheme shows that ALDH1$^+$ WT cells retain their CSC phenotype in pure blastema Xns. Pure blastema Xns were sorted according to ALDH1 activity. ALDH1$^+$ and ALDH1$^-$ blastemal cells were then injected into mice. Only ALDH1$^+$ cells were able to initiate tumors in all dilutions applied, whereas ALDH1$^-$ cells failed to form tumors altogether. Following ALDH1$^+$-derived tumor growth, sorting and injections of ALDH1$^+$ and ALDH1$^-$ cells were repeated with equivalent results, confirming that ALDH1$^+$ cells maintain self-renewal capacity in pure blastema Xns.

(B) Representative FACS analysis of untreated Xn cells in comparison to Xn cells treated with ionizing radiation at an intensity of 10 Gy reveals enrichment of ALDH1$^+$ population.

(legend continued on next page)

of rapamycin [mTOR]) (Table S1). Thus, pure blastema WT Xns, enriched for ALDH1$^+$ CSCs, demonstrate a more epithelial phenotype than their US-derived counterparts, while maintaining their stemness. We next determined whether culture conditions of pure blastema Xn cells can recapitulate in vivo findings. We employed low-attachment conditions to grow CSC-En tumor spheres (Yano et al., 2013) and interrogated their phenotype by comparison to adherent culture. Tumor spheres demonstrated high ALDH1 expression, accompanied by high expression of stemness genes (e.g., *OCT4*, *NANOG*, and Polycomb genes) and skewing toward a more epithelial phenotype (i.e., lower *SIX2*, *OSR1*, *CITED1*, *vimentin*, and higher *E-Cadherin* and *EpCAM* levels) (Figure 3E). Thus, altering culture conditions to enrich for CSCs can result in a relative renal MET, mirroring the in vivo state.

Global Gene Analysis Reveals that WT CSC Is Arrested at a Renal Progenitor State, Committed to Epithelial Differentiation

We next sought to characterize the molecular profile of the ALDH1$^+$ CSCs. For this purpose, we performed a microarray gene expression analysis comparing three samples: (1) sorted ALDH1$^+$ cells, (2) sorted ALDH1$^-$ cells, and (3) USs. This comparison revealed a unique gene expression profile of the ALDH1$^+$ CSCs that included high levels of stemness genes (e.g., *OCT4*, *SHH*, *LIN28A*, and *KLF4*) and relatively high levels of epithelial markers (e.g., Keratin 6c, Keratin 33a, Keratin 35, Claudin 7, Claudin 9, and Claudin 13) alongside lower levels of mesenchymal markers (e.g., vimentin, *SNAI2*, and *MEST*) (Figures 4A and S3). Importantly, ALDH1$^+$ cells demonstrated lower levels of proliferation-related genes (e.g., *PCNA*, *CCNB1*, and *E2F1*) compared to ALDH1$^-$ cells, suggesting a more quiescent phenotype of this population (Figure 4A). In order to validate the microarray data, quantitative real-time PCR was performed on sorted ALDH1$^+$ and ALDH1$^-$ cells derived from three different pure blastema WT Xn sources. Characterization of these fractions demonstrated that indeed ALDH1$^+$ cells express lower levels of renal developmental genes (Figure 4B). Moreover, higher E-Cadherin and lower vimentin expression in ALDH1$^+$ cells was noted in comparison to ALDH1$^-$ cells (Figure 4B). In order to further evaluate the proliferative state of the different factions within the pure blastema WT Xns, we carried out flow cytometry cell-cycle analysis. In accordance with the microarray data, the ALDH1$^+$ fraction demonstrated a higher percentage of cells in the G0/G1 phase compared to USs (87.4% and 75.8%, respectively) (Figure S4). We next characterized ALDH1$^+$ cells at the protein level. We performed western blot analysis of renal MET protein expression comparing four samples: (1) sorted ALDH1$^+$ Xn cells, (2) sorted ALDH1$^-$ Xn cells, (3) unsorted Xn cells, and (4) primary WT (pWT). The results demonstrated lower expression of SIX2 and higher expression of E-Cadherin in ALDH1$^+$ cells (Figure 4C). Interestingly, pWT presented higher E-Cadherin levels and lower vimentin and SIX2 levels compared to the Xn samples, emphasizing the mesenchymal, undifferentiated nature of the blastema-pure tumors. In addition, immunofluorescence (IF) staining of sorted ALDH1$^+$ and ALDH1$^-$ WT Xn cells for SIX2 and the epithelial markers E-Cadherin and cytokeratin (MNF 116) showed distinct staining patterns. ALDH1$^+$ cells presented significantly lower expression of SIX2 (Figure 4D, left) and higher expression of epithelial markers (Figure 4D, middle and right). Furthermore, in order to demonstrate in vitro dedifferentiation capacity of the ALDH1$^+$ sorted fraction, cells were grown in culture for 10 days. We observed the acquisition of a mesenchymal phenotype, as manifested by upregulation of vimentin alongside downregulation of ALDH1 expression and the epithelial markers E-Cadherin and EpCAM (Figure 4E). Taken together, these results suggest that the WT CSCs are not the least differentiated cells along the renal developmental MET axis but, rather, are arrested at a renal progenitor state, committed to epithelial differentiation. Thus, the WT CSCs are likely to dedifferentiate to propagate WT blastema.

DISCUSSION

Here, by comparing the WT CSCs with normal kidney development, we discover two surprising fundamental concepts. First, in terms of lineage hierarchy, the CSC may not correspond to the earliest normal stem cell but rather to a more differentiated progeny. Second, heterogeneity that mirrors renal stem cell differentiation is present in the homogeneous-appearing WT blastema. Our earlier observations (Pode-Shakked et al., 2013) disclosed high similarity between WT CSCs and early renal stem cells. These observations were based on propagation of trilineage human WT, in which the relationship of the CSC to tumor bulk includes a comparison to blastema and also to mature elements, placing the CSC as an undifferentiated renal cell type. Our ability to examine pure blastema Xns enabled

(C) Summary of ionizing radiation effect on proliferation and ALDH1 expression of Xn cells. Left view shows that ionizing radiation inhibits cell growth in a dose- and time-dependent manner. Right view shows that exposure of WT Xn cells to ionizing radiation enriches for the ALDH1$^+$ CSC population in a dose- and time-dependent manner.
See also Figure S2.

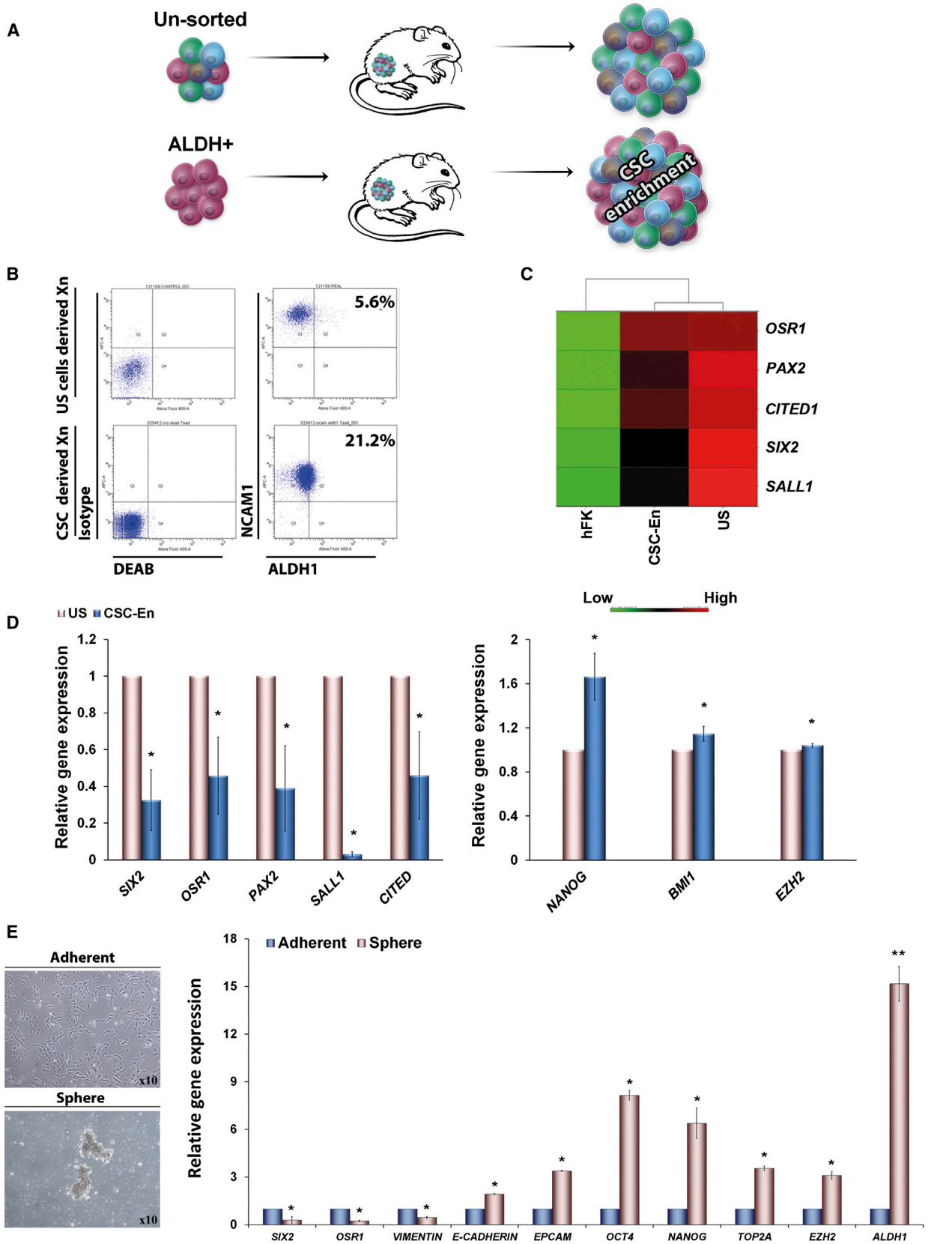

(legend on next page)

stringent comparison of WT CSCs to the undifferentiated tumor bulk and the unraveling of the findings. Indeed, the importance of the fine-tuning of our system is manifested when comparing WT CSCs to parental tissues (i.e., hFK and pWT), disclosing a relatively undifferentiated phenotype. This precise understanding of the relation between the WT CSC and embryonic renal differentiation affords insights from both oncologic and developmental aspects. Multiple studies have highlighted the relationship between CSCs and their differentiated progeny (Reya et al., 2001), including WT CSCs, and their ability to generate tubular structures and glomeruloid bodies (Little, 2005; Pode-Shakked and Dekel, 2011; Pode-Shakked et al., 2013). Nevertheless, the dedifferentiated progeny arising from ALDH1$^+$ WT CSCs, represented by the bulk of the blastema and characterized by higher SIX2 and lower E-Cadherin, illustrates mechanisms for WT and progression. Interestingly, partial reprogramming by pluripotent stemness factors has been recently implicated in generation of a Wilms'-like tumor in vivo (Ohnishi et al., 2014). Hypothetically, dedifferentiation of WT CSCs may also account for the nonrenal mesenchymal elements observed in WT. This notion is strengthened by the fact that developmental lineages are already specified in the MM, and no common nephron epithelial-stromal progenitor cell has been documented (Brown et al., 2013; Kobayashi et al., 2008; Pleniceanu et al., 2010; Self et al, 2006). Our work may suggest a revision to the concept that the earliest transformed renal stem cell capable of giving rise to differentiated progeny is the tumor-initiating cell. Alternatively, the WT cell of origin and WT CSCs responsible for tumor propagation may not be the same cell. Resolution of this matter utilizing a transgenic animal model of WT generation that employs specific CRE drivers of renal stem cells (e.g., *SIX2*) might be complicated because WT CSCs express some levels of *SIX2* and *WT1*. Finally, from the developmental aspect, it remains to be determined how NCAM1$^+$ human nephron progenitors isolated from the hFK and representing more committed epithelial progenitors than uninduced MM (Harari-Steinberg et al., 2013) are relevant for WT once transformed.

From a more practical aspect, the unequivocal limiting-dilution xenotransplantation data, illustrating ALDH1$^+$ WT CSCs as critical for continued propagation of WT blastema Xns, highlight the WT CSC as a therapeutic target. We previously suggested anti-NCAM1-targeted therapy as a useful means for WT eradication (Pode-Shakked et al., 2013). Clearly, the NCAM1 expression domain exceeds that of the WT CSC. In this regard, our genomic and proteomic data disclose several specific pathways (e.g., NF-κB, Wnt, PI3K, and mTOR) previously implicated in stemness acquisition (Armstrong et al., 2006; Huang et al., 2012; Katoh and Katoh, 2007; Shostak and Chariot, 2011) as highly operative in WT CSCs. Thus, global analysis not only sheds light on the WT CSC as possessing enhanced stemness alongside a more differentiated renal phenotype but also pinpoints interventions such as mTOR and epidermal growth factor receptor inhibition that may prove beneficial in WT CSC eradication.

EXPERIMENTAL PROCEDURES

Detailed Experimental Procedures are provided in the Supplemental Experimental Procedures.

pWT Samples

pWT samples were obtained from patients with WT within 1 hr of surgery from both Sheba Medical Center and Hadassah-EinKerem hospital. All studies were approved by the local ethics committee,

Figure 3. Analysis of WT CSC Fraction in Relation with Renal MET Axis Reveals Developmental Heterogeneity in WT Blastema

(A) Scheme presents WT Xns derived from ALDH1$^+$ sorted cells (bottom) that show enrichment in ALDH1$^+$ CSCs in comparison with pure blastema WT Xns derived from USs (top).

(B) Representative FACS analyses of WT Xns derived from either unsorted WT cells (top) or ALDH1$^+$ WT cells (bottom) showing enrichment in ALDH1$^+$ WT CSCs in the latter.

(C) Gene heatmap of pure blastema CSC-En tumors in comparison to US-derived Xn and hFK. This analysis revealed that the CSC-En Xn and, to an even greater extent, the Xn derived from USs are enriched for the earliest renal developmental gene set in comparison to the hFK.

(D) Validation via quantitative real-time PCR of renal developmental genes (i.e., *WT1*, *SIX2*, *SALL1*, *OSR1*, *CITED1*, and *PAX2*) (left) and stemness genes (i.e., *NANOG*, *BMI1*, and *EZH2*) (right) in unsorted and CSC-En Xns. For quantitative real-time PCR analyses, the values for unsorted-derived pure blastema WT Xn cells were used to normalize (therefore equaling one [1]), and all other values were calculated with respect to them. Results are presented as the mean ± SEM of five separate experiments obtained from three different patients. *$p < 0.05$.

(E) Unsorted Xn cells were grown in two different culture conditions (images by light microscopy are shown on the left): adherent cells (top), and sphere-forming cells, grown in low-attachment conditions (bottom). The spheres demonstrated high *ALDH1* expression accompanied by high levels of stemness genes (i.e., *OCT4*, *NANOG*, *TOP2A*, and *EZH2*) along with a more epithelial phenotype (lower levels of *SIX2*, *OSR1*, *CITED1*, and *vimentin* and higher levels of *E-Cadherin* and *EpCAM*). The values for adherent cells were used to normalize (therefore equaling one [1]), and other values were calculated with respect to them. Results are presented as the mean ± SEM of three separate experiments. *$p < 0.05$; **$p < 0.01$.

See also Figure S2 and Tables S1 and S2.

A

Function	ID	Gene Symbol	ALDH1+ vs. ALDH1-
Cell proliferation	11723713_at	*E2F1*	0.62
	11760225_at	*PLK1S1*	0.55
	11732997_a_at	*MCM6*	0.52
	11720971_at	*TOP2A*	0.50
	11744169_a_at	*MYBL2*	0.45
	11759510_x_at	*MCM4*	0.44
	11723939_a_at	*CCNB1*	0.43
	11756666_x_at	*MCM2*	0.34
	11747230_a_at	*BUB1*	0.30
	11716103_a_at	*PCNA*	0.23
	11724407_s_at	*CCNE1*	0.23
	11742996_a_at	*MCM3*	0.11
Renal patterninig	11725907_at	*SIX2*	0.18
	11724865_at	*OSR1*	0.44
	11732702_a_at	*CITED1*	0.55
	11728563_at	*FOXD1*	0.49
	11728624_a_at	*PAX2*	0.70
Stemness	11738265_at	*SHH*	6.26
	11755599_x_at	*POU5F1*	1.65
	11725430_at	*LIN28A*	1.96
	11719633_a_at	*KLF4*	2.40
MET/EMT	11731342_at	*CLDN9*	2.30
	11739907_at	*CLDN16*	1.87
	11727492_at	*KRT6C*	5.45
	11738651_at	*KRT35*	4.84
	11715296_s_at	*KRT33A*	3.28
	11755943_x_at	*VIM*	0.63
	11744985_a_at	*FNDC3A*	0.53
	11744218_at	*SNAI2*	0.22
	11754365_s_at	*ROR2*	0.04
	11723029_x_at	*MEST*	0.23
	11716195_a_at	*ID1*	0.57

B

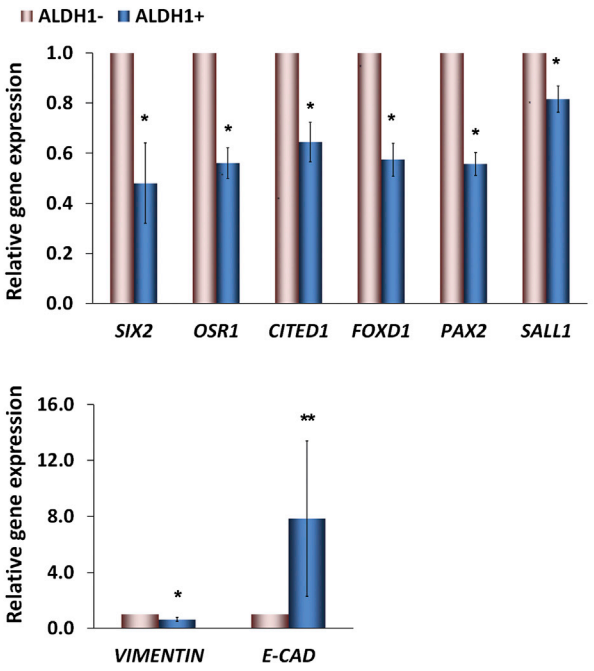

C

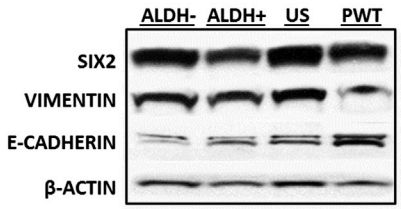

D

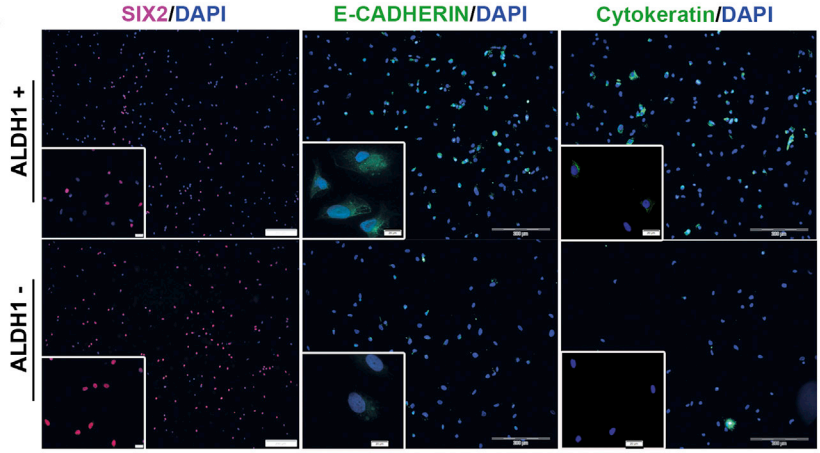

E

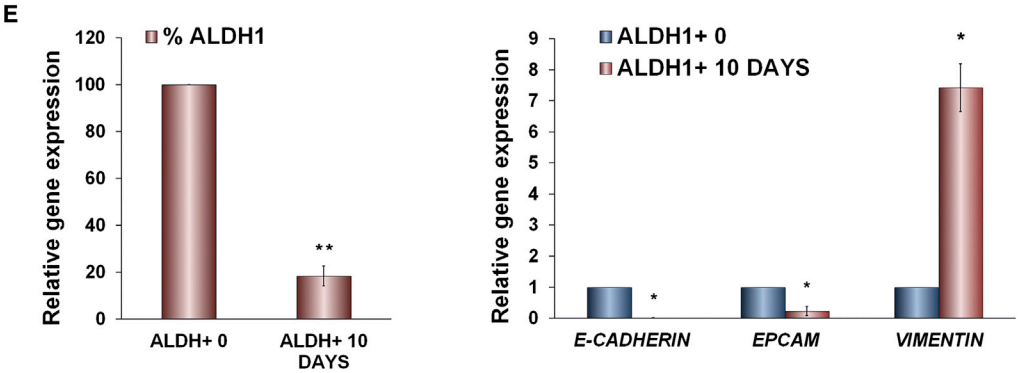

(legend on next page)

and informed consent was given by the legal guardians of the patients involved according to the Declaration of Helsinki.

In Vivo Xn Formation

The animal experiments were performed in accordance with the Guidelines for Animal Experiments of Sheba Medical Center. Initial WT xenografting to 5- to 8-week-old, female, nonobese diabetic severe combined immunodeficiency (NOD-SCID) mice was performed as previously described (Dekel et al., 2006). Late-passage Xns were formed by serial injections of approximately 10^6 dissociated cells from freshly retrieved WT Xns. Cells were injected in 100 μl 1:1 serum-free medium/Matrigel (BD Biosciences). See also Supplemental Experimental Procedures.

Statistical Analysis

Results are expressed as the mean ± SEM, unless otherwise indicated. Statistical differences in gene expression between WT cell populations were evaluated using the nonparametric, one-sided sign test. Statistical differences between additional data groups were determined with Student's t test. For all statistical analyses, the level of significance was set as $p < 0.05$, unless otherwise indicated.

ACCESSION NUMBERS

The GEO accession number for the chromatin immunoprecipitation array data reported in this paper is GSE57269.

SUPPLEMENTAL INFORMATION

Supplemental Information includes Supplemental Experimental Procedures, four figures, and three tables and can be found with this article online at http://dx.doi.org/10.1016/j.stemcr.2014.05.013.

AUTHOR CONTRIBUTIONS

B.D., R.S., and N.P.-S. designed the experiments. R.S. and S.P.-C. performed the in vivo experiments. R.S., E.P., E.V., Q.H., V.H., O.H.-S., and D.O. performed in vitro assays. B.D., J.J., R.S., and N.P.-S. analyzed the data. B.D., R.S., O.P., and N.P.-S. wrote the manuscript.

ACKNOWLEDGMENTS

We thank Itamar Goldstein for his assistance with the FACS experiments, Peter Hohenstein for critically reading the manuscript, and Yaacov Lawrence for assisting with the ionizing radiation experiments. This work was supported by the MD Anderson Global Academic Programs (to B.D. and V.H.), The Zeiring Foundation, and The Israel Cancer Fund (Grant number PG-11-3072 to B.D.). This work is part of the requirements toward a PhD degree at the Sackler School of Medicine, Tel Aviv University (for R.S.).

Received: November 20, 2013
Revised: May 18, 2014
Accepted: May 19, 2014
Published: June 26, 2014

REFERENCES

Armstrong, L., Hughes, O., Yung, S., Hyslop, L., Stewart, R., Wappler, I., Peters, H., Walter, T., Stojkovic, P., Evans, J., et al. (2006). The role of PI3K/AKT, MAPK/ERK and NFkappabeta signalling in the maintenance of human embryonic stem cell pluripotency and viability highlighted by transcriptional profiling and functional analysis. Hum. Mol. Genet. *15*, 1894–1913.

Figure 4. Global Analysis Reveals a Distinct Profile of CSCs Congruent with MET and Not Uninduced Mesenchymal Progenitors

Molecular profile analyses of WT ALDH1$^+$ CSCs.

(A) Microarray gene expression analysis of WT CSCs. A table is shown of gene expression fold change comparing sorted ALDH1$^+$ and ALDH1$^-$ cells. ALDH1$^+$ CSCs demonstrate low levels of proliferation-related genes (e.g., *PCNA*, *CCNB1*, and *E2F1*), lower levels of renal developmental genes (e.g., *SIX2*, *OSR1*, and *CITED1*), high levels of stemness genes (e.g., *POU5F1*, *SHH*, *LIN28A*, and *KLF4*), high expression of epithelial markers (*E-Cadherin*, *Keratin 6c*, *Keratin 33a*, *Keratin 35*, *Claudin 7*, *Claudin 9*, and *Claudin 13*), and lower levels of mesenchymal markers (*vimentin*, *SNAI2*, and *MEST*).

(B) Quantitative real-time PCR demonstrating significantly reduced levels of renal-patterning genes (i.e., *SIX2*, *OSR1*, *CITED1*, *SALL1*, and *PAX2*) along with elevation of *E-Cadherin* (*E-CAD*) and decreased *vimentin* in ALDH1$^+$ cells. The values for ALDH1$^-$ WT cells were used to normalize (therefore equaling one [1]), and all other values were calculated with respect to them. Results are presented as the mean ± SEM of five separate experiments obtained from three different patients. *$p < 0.05$; **$p < 0.01$.

(C) Western blot analysis of renal MET protein expression in four samples: (1) ALDH1$^+$ cells, (2) ALDH1$^-$ cells, (3) USs, and (4) pWT cells. This analysis demonstrated lower expression of SIX2 and higher expression of E-Cadherin in ALDH1$^+$ in comparison with ALDH1$^-$ WT cells. In addition, pWT cells present higher levels of E-Cadherin and lower levels of vimentin and SIX2 in comparison to the Xn samples, emphasizing the mesenchymal nature of the blastema-pure tissues.

(D) IF staining of sorted ALDH1$^+$ and ALDH1$^-$ WT Xn cells for SIX2 (left panel) and the epithelial markers: E-Cadherin (middle panel) and cytokeratin (right panel). A distinct staining pattern showing higher protein expression of the epithelial markers and lower expression of SIX2 in ALDH1$^+$ in comparison with ALDH1$^-$ cells can be seen. Scale bars, 200 μm.

(E) ALDH1$^+$ sorted cells were grown for 10 days in culture. Gene expression comparison of noncultured cells (ALDH$^+$ 0) and cultured cells (ALDH$^+$ 10 days) revealed significant downregulation of *ALDH1* expression (left) and upregulation of *vimentin* alongside downregulation of the epithelial markers *E-Cadherin* and *EpCAM* (right), demonstrating plasticity of the ALDH1$^+$ CSCs. The values for ALDH$^+$ 0 cells were used to normalize (therefore equaling one [1]), and all other values were calculated with respect to them. Results are presented as the mean ± SEM of three separate experiments. *$p < 0.05$; **$p < 0.01$.

See also Figures S3 and S4 and Table S3.

Bonnet, D., and Dick, J.E. (1997). Human acute myeloid leukemia is organized as a hierarchy that originates from a primitive hematopoietic cell. Nat. Med. *3*, 730–737.

Brown, A.C., Muthukrishnan, S.D., Guay, J.A., Adams, D.C., Schafer, D.A., Fetting, J.L., and Oxburgh, L. (2013). Role for compartmentalization in nephron progenitor differentiation. Proc. Natl. Acad. Sci. USA *110*, 4640–4645.

Cirio, M.C., de Groh, E.D., de Caestecker, M.P., Davidson, A.J., and Hukriede, N.A. (2014). Kidney regeneration: common themes from the embryo to the adult. Pediatr. Nephrol. *29*, 553–564.

Dekel, B., Metsuyanim, S., Schmidt-Ott, K.M., Fridman, E., Jacob-Hirsch, J., Simon, A., Pinthus, J., Mor, Y., Barasch, J., Amariglio, N., et al. (2006). Multiple imprinted and stemness genes provide a link between normal and tumor progenitor cells of the developing human kidney. Cancer Res. *66*, 6040–6049.

Dekel, B., Metsuyanim, S., Goldstein, N., Pode-Shakked, N., Kovalski, Y., Cohen, Y., Davidovits, M., and Anikster, Y. (2008). Schimke immuno-osseous dysplasia: expression of SMARCAL1 in blood and kidney provides novel insight into disease phenotype. Pediatr. Res. *63*, 398–403.

Harari-Steinberg, O., Metsuyanim, S., Omer, D., Gnatek, Y., Gershon, R., Pri-Chen, S., Ozdemir, D.D., Lerenthal, Y., Noiman, T., Ben-Hur, H., et al. (2013). Identification of human nephron progenitors capable of generation of kidney structures and functional repair of chronic renal disease. EMBO Mol. Med. *5*, 1556–1568.

Huang, J., Nguyen-McCarty, M., Hexner, E.O., Danet-Desnoyers, G., and Klein, P.S. (2012). Maintenance of hematopoietic stem cells through regulation of Wnt and mTOR pathways. Nat. Med. *18*, 1778–1785.

Katoh, M., and Katoh, M. (2007). WNT signaling pathway and stem cell signaling network. Clin. Cancer Res. *13*, 4042–4045.

Kobayashi, A., Valerius, M.T., Mugford, J.W., Carroll, T.J., Self, M., Oliver, G., and McMahon, A.P. (2008). Six2 defines and regulates a multipotent self-renewing nephron progenitor population throughout mammalian kidney development. Cell Stem Cell *3*, 169–181.

Li, C.M., Guo, M., Borczuk, A., Powell, C.A., Wei, M., Thaker, H.M., Friedman, R., Klein, U., and Tycko, B. (2002). Gene expression in Wilms' tumor mimics the earliest committed stage in the metanephric mesenchymal-epithelial transition. Am. J. Pathol. *160*, 2181–2190.

Little, M. (2005). Wilms' tumor: starting off the kidney all over again? Prog. Mol. Subcell. Biol. *40*, 107–132.

Metsuyanim, S., Harari-Steinberg, O., Buzhor, E., Omer, D., Pode-Shakked, N., Ben-Hur, H., Halperin, R., Schneider, D., and Dekel, B. (2009). Expression of stem cell markers in the human fetal kidney. PLoS One *4*, e6709.

Ohnishi, K., Semi, K., Yamamoto, T., Shimizu, M., Tanaka, A., Mitsunaga, K., Okita, K., Osafune, K., Arioka, Y., Maeda, T., et al. (2014). Premature termination of reprogramming in vivo leads to cancer development through altered epigenetic regulation. Cell *156*, 663–677.

Pleniceanu, O., Harari-Steinberg, O., and Dekel, B. (2010). Concise review: kidney stem/progenitor cells: differentiate, sort out, or reprogram? Stem Cells *28*, 1649–1660.

Pode-Shakked, N., and Dekel, B. (2011). Wilms tumor—a renal stem cell malignancy? Pediatr. Nephrol. *26*, 1535–1543.

Pode-Shakked, N., Shukrun, R., Mark-Danieli, M., Tsvetkov, P., Bahar, S., Pri-Chen, S., Goldstein, R.S., Rom-Gross, E., Mor, Y., Fridman, E., et al. (2013). The isolation and characterization of renal cancer initiating cells from human Wilms' tumour xenografts unveils new therapeutic targets. EMBO Mol. Med. *5*, 18–37.

Reya, T., Morrison, S.J., Clarke, M.F., and Weissman, I.L. (2001). Stem cells, cancer, and cancer stem cells. Nature *414*, 105–111.

Rivera, M.N., and Haber, D.A. (2005). Wilms' tumour: connecting tumorigenesis and organ development in the kidney. Nature reviews *5*, 699–712.

Royer-Pokora, B., Busch, M., Beier, M., Duhme, C., de Torres, C., Mora, J., Brandt, A., and Royer, H.D. (2010). Wilms tumor cells with WT1 mutations have characteristic features of mesenchymal stem cells and express molecular markers of paraxial mesoderm. Hum. Mol. Genet. *19*, 1651–1668.

Self, M., Lagutin, O.V., Bowling, B., Hendrix, J., Cai, Y., Dressler, G.R., and Oliver, G. (2006). Six2 is required for suppression of nephrogenesis and progenitor renewal in the developing kidney. EMBO J. *25*, 5214–5228.

Shostak, K., and Chariot, A. (2011). NF-κB, stem cells and breast cancer: the links get stronger. Breast Cancer Res. *13*, 214.

Shukrun, R., Pode Shakked, N., and Dekel, B. (2014). Targeted therapy aimed at cancer stem cells: Wilms' tumor as an example. Pediatr. Nephrol. *29*, 815–823.

Yano, S., Tazawa, H., Hashimoto, Y., Shirakawa, Y., Kuroda, S., Nishizaki, M., Kishimoto, H., Uno, F., Nagasaka, T., Urata, Y., et al. (2013). A genetically engineered oncolytic adenovirus decoys and lethally traps quiescent cancer stem-like cells in S/G2/M phases. Clin. Cancer Res. *19*, 6495–6505.

Stem Cell Reports, Volume *3*

Supplemental Information

Wilms' Tumor Blastemal Stem Cells Dedifferentiate to Propagate the Tumor Bulk

Rachel Shukrun, Naomi Pode-Shakked, Oren Pleniceanu, Dorit Omer, Einav Vax, Eyal Peer, Sara Pri-Chen, Jasmine Jacob, Qianghua Hu, Orit Harari-Steinberg, Vicki Huff, and Benjamin Dekel

Supplemental figures and figure legends

Figure S1: NCAM1, SIX2 and ALDH1 expression in WT Xn

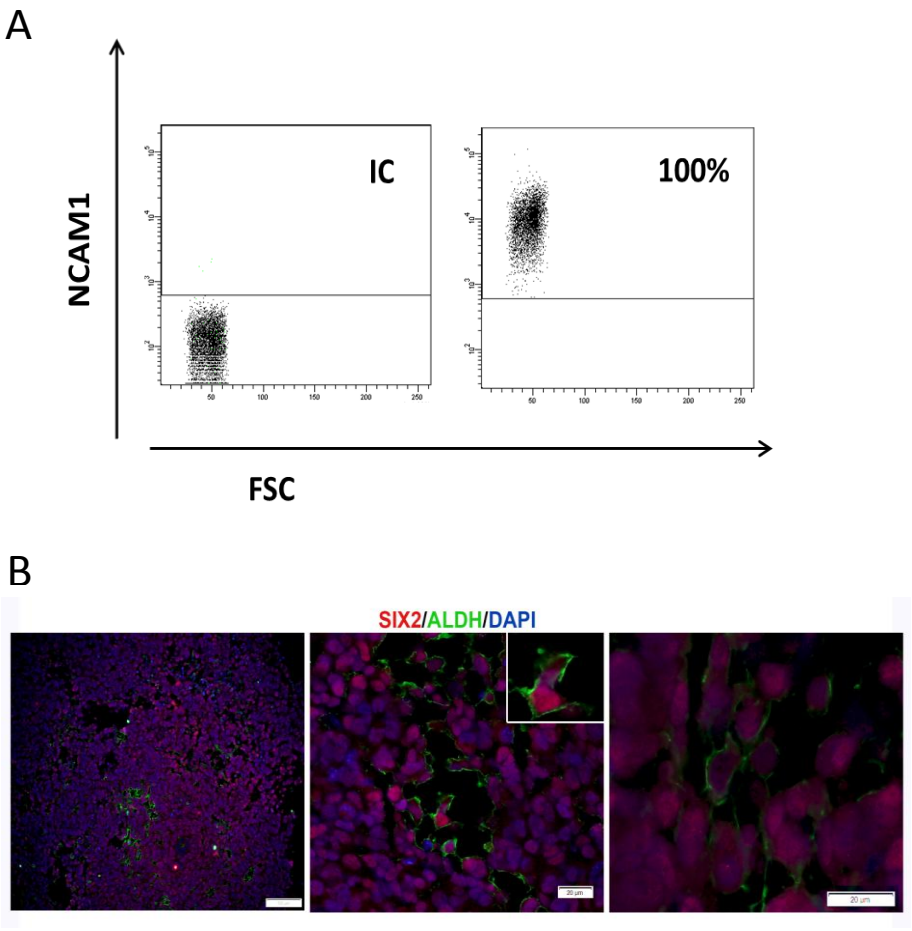

(A) All late WT Xn cells express high levels of NCAM1. FACS analysis of late WT Xn cells, demonstrating high expression of NCAM1 in all tumor cells, emphasizing that late Xn are composed solely of blastemal cells. IC, Isotype control.

(B) SIX2 and ALDH1are both expressed by the WT CSC. Immuno-fluorescent staining of pure-blastema WT Xn for SIX2 (red), ALDH1 (green) and DAPI nuclear staining (blue). All the tumor cells are SIX2+ while ALDH1+ cells are scattered within these blastemal sheets. Scale bar; 100µm (left panel), 20µm (middle and right panels).

Figure S2: Validation of ALDH1 gene expression levels

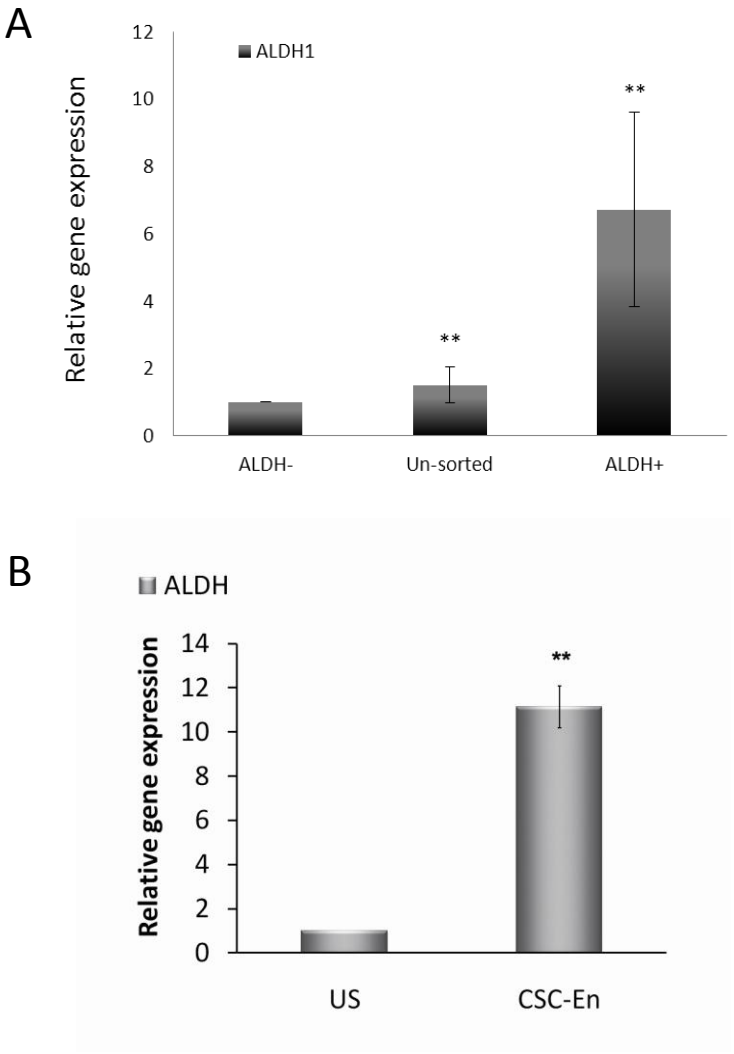

(A) Validation of ALDH1 FACS-sorting quality. Quantitative real-time PCR analysis of *ALDH1* expression levels following FACS-sorting according to ALDH1 enzymatic activity, confirming high efficiency enrichment of ALDH1+ cells. The values for ALDH1- cells were used to normalize (therefore=1) and all other values were calculated with respect to them. Results are presented as the mean ± S.E.M of three separate experiments; **, $p<0.01$

(B) Validation of ALDH1 expression in the different Xn models. Validation via qRT-PCR of ALDH1 expression in un-sorted derived (US) and ALDH1+ derived (CSC-En) Xn, showing up-regulation in the latter. Results are presented as the mean ±SEM of experiments obtained from three different patients; ** $p<0.01$

Figure S3: microarray gene expression analysis

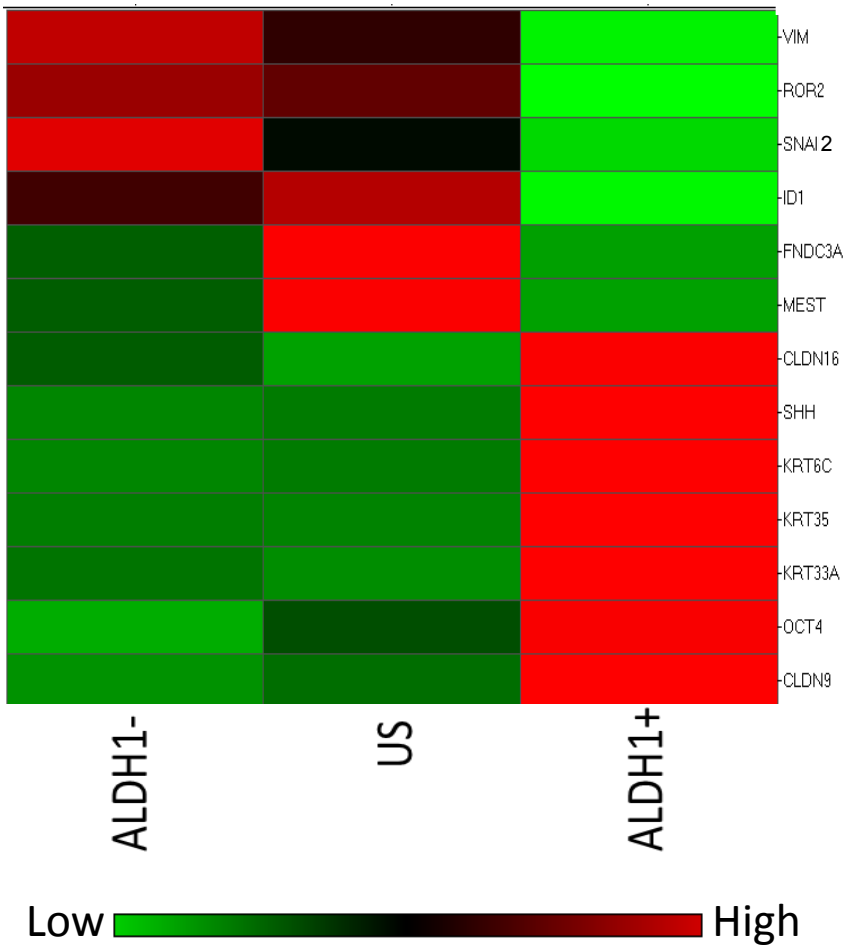

Microarray gene expression analysis of WT CSCs. Representative Heat map of differentially expressed genes between: 1. sorted ALDH+ cells, 2. sorted ALDH- cells and 3. Un-sorted Xn cells (US). This comparison revealed a unique profile of the ALDH+ CSCs including high levels of stemness genes (*OCT4 and SHH*), along with high expression of epithelial differentiation markers (*E-Cadherin, Keratin 6c,33a,35 and Claudine 7,9,13*) and lower levels of mesenchymal markers (*Vimentin, SNAI2, MEST*).

Figure S4: ALDH+ WT CSC present a quiescent nature

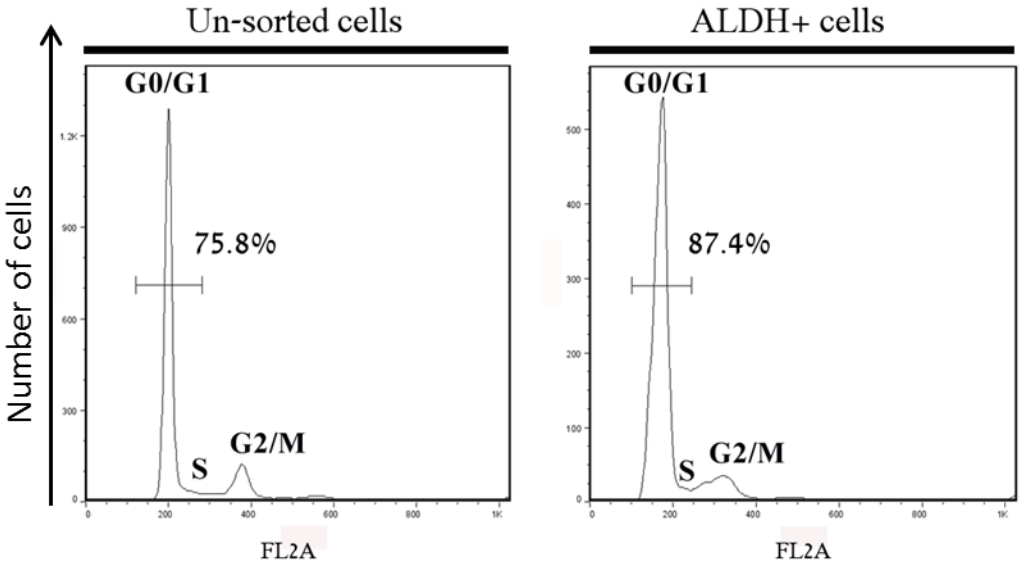

Reprehensive flow cytometric cell cycle analysis revealed that the ALDH1+ fraction demonstrated a higher percentage of cells in the G0/G1 phase compared to unsorted cells (87.4% and 75.8%, respectively), further supporting their quiescent nature.

Supplemental tables

Table S1| Proteomic analysis of ALDH1+ CSC enriched WT Xn:

Proteins up-regulated in ALDH1$^+$ CSC enriched WT xenografts		
Function/Pathway WT cells	**Gene symbol**	**Protein name**
MET (Epithelial)	*CDH1, EGFR*	E-Cadherin; EGFR_pY1068, EGFR
Stemness (self renewal, hESC)	*NOTCH1*	Notch1
NFκB/Akt pathway	*AKT1, AKT2 AKT3; NFKB1*	Akt_pS473; NF-kB-p65_pS536;
Wnt/beta catenin pathway	*GSK3A, GSK3B*	GSK3-alpha-beta
PI3K/PKC pathway	*PIK3CA; PIK3R1; PRKCA*	PI3K-p85; PI3K-p110-alpha; PKC-alpha
mTOR signaling pathway	*TSC1*	TSC1
Onco-proteins	*RAF1; SRC; EGFR; CCNB1*	C-Raf; Src_pY527, Src; EGFR; EGFR_pY1068; Cyclin_B1
Tumor suppressor proteins	*RB1; SMAD3;*	Rb_pS807_S811 ; TAZ
Proteins down-regulated in ALDH1+ CSC enriched WT xenografts		
Function/pathway	**Gene symbol**	**Protein name**
MET (Mesenchymal)	*COL6A1; SNAI2*	Collagen VI; Snai2
Endothelial	*PECAM1*	CD31
DNA repair genes	*RAD50*	Rad50
Proliferation	*PCNA*	PCNA
Onco-proteins	*YAP1, ; WWTR1 RAB25; MET*	YAP; WWTR1; Rab25; c-Met_pY1235
Tumor suppressor proteins	*CAV1*	Caveolin-1

Shown are up-regulated (upper panel) and down-regulated (lower panel) proteins, according to their ascribed function.

Table S2| 10 most up- and down-regulated genes in CSC-En Xn in comparison to un-sorted derived Xn and human fetal kidney (hFK):

10 most up-regulated genes in CSC-En Xn in comparison to un-sorted derived Xn and human fetal kidney (hFK):

	Gene Symbol	Gene Title	Un-derived Xn	CSC-En Xn	hFK
1	*GPR89B/C*	G protein-coupled receptor 89B/C	7.9	98.5	15.4
2	*GFRAL*	GDNF family receptor alpha like	7.7	57.9	4.1
3	*C6orf115*	chromosome 6 open reading frame 115	5.3	37.7	42.0
4	*COL6A5*	collagen, type VI, alpha 5	10.2	44.4	4.1
5	*IGHV7-81*	immunoglobulin heavy variable 7-81	5.2	18.0	4.6
6	*THBS4*	thrombospondin 4	62.8	211.5	10.4
7	*FOXF1*	forkhead box F1	4.6	14.7	4.7
8	*SNORA33*	small nucleolar RNA, H/ACA box 33	4.8	14.9	9.5
9	*SHH*	sonic hedgehog	5.7	16.1	5.3
10	*XKR9*	XK, Kell blood group complex subunit, member 9	157.5	429.8	4.8

10 most down-regulated genes in CSC-En Xn in comparison to un-sorted derived Xn and human fetal kidney (hFK):

1	*PCBP4*	poly(rC) binding protein 4	99.0	22.1	28.3
2	*NPY*	neuropeptide Y	361.0	109.0	5.3
3	*LGALS1*	lectin, galactoside-binding, soluble, 1	30.3	9.2	333.2
4	*GTF2B*	general transcription factor IIB	109.3	37.3	129.4
5	*ALDOA*	aldolase A, fructose-bisphosphate	22.6	7.8	152.5
6	*MANF*	mesencephalic astrocyte-derived neurotrophic factor	27.9	10.4	176.1
7	*UGP2*	UDP-glucose pyrophosphorylase 2	30.6	11.4	221.0
8	*RNF20*	ring finger protein 20	12.5	4.9	98.3
9	*ENO1*	enolase 1, (alpha)	416.7	164.1	227.7
10	*ETV5*	ets variant 5	215.5	85.7	13.4

Table S3| 10 most up- and down-regulated genes in ALDH+ in comparison to ALDH- and un-sorted Xn cells:

10 most up-regulated genes in ALDH+ in comparison to ALDH- and un-sorted Xn cells:

	Gene Symbol	Gene Title	ALDH+	ALDH-	US
1	*BNIP3L*	BCL2/adenovirus E1B 19kDa interacting protein 3-like	106.0	7.8	11.2
2	*HSD17B8*	hydroxysteroid (17-beta) dehydrogenase 8	51.9	5.2	4.2
3	*NUDT16*	nudix-type motif 16	52.7	5.6	53.9
4	*ACPL2*	acid phosphatase-like 2	41.3	4.7	4.9
5	*PABPC1L2A*	poly(A) binding protein, cytoplasmic 1-like 2A	65.0	7.7	5.1
6	*TRIM33*	tripartite motif-containing 33	151.6	18.2	91.4
7	*LOC100128185*	PNAS-19	58.8	7.4	4.5
8	*C6orf25*	chromosome 6 open reading frame 25	38.3	5.7	16.7
9	*GP1BA*	glycoprotein Ib (platelet), alpha polypeptide	30.0	4.8	5.5

10 most down-regulated genes in ALDH+ in comparison to ALDH- and un-sorted Xn cells:

1	*DAOA-AS*	DAOA antisense RNA (non-protein coding)	7.0	191.2	144.0
2	*PTTG1/3P*	pituitary tumor-transforming 1/3	23.2	569.4	826.7
3	*CTRB2*	chymotrypsinogen B2	5.9	143.9	188.5
4	*IGSF21*	immunoglobin superfamily, member 21	8.8	170.0	153.2
5	*DNMT3L*	DNA (cytosine-5-)-methyltransferase 3-like	16.8	320.2	292.2
6	*NME1*	non-metastatic cells 1, protein (NM23A)	6.6	122.4	176.6
7	*CHST1*	carbohydrate (keratan sulfate Gal-6) sulfotransferase 1	9.1	160.7	268.4
8	*ANKRD36*	ankyrin repeat domain 36	5.5	92.1	81.3
9	*ECHDC3*	enoyl CoA hydratase domain containing 3	18.6	309.6	453.3
10	*LETMD1*	LETM1 domain containing 1	11.5	184.3	182.1

Supplemental experimental procedures

Ethics statement

This study was conducted according to the principles expressed in the Declaration of Helsinki and was approved by the Institutional Review Boards of Sheba, Hadassah-Ein Kerem and Asaf Harofeh Medical Centers.

In vivo xenograft formation

Initial WT xenografting to 5-8 weeks old, female, nonobese diabetic immunodeficient mice v mice was performed as previously described (15). Briefly, primary WT tissue was cut into 2-5mm pieces and implanted subcutaneously in the back of the mouse. Tumors were harvested approximately 3-6 month post implantation or when they reached a size of 1.5cm diameter. Single cells suspensions were obtained by mincing the samples in Iscove's modification of Dulbecco's medium (IMDM) containing antibiotics (penicillin and streptomycin), followed by treatment with collagenase IV for 2h at 37◦C. Enzymatically treated tissue was triturated using IMDM at twice the volume of the collagenase solution and the suspension filtered (100μm cell strainer) and washed twice with IMDM containing antibiotics. Erythrocytes were removed by ACK RBS lysis buffer.

Late passages Xn were formed by serial injection of approximately 106 dissociated cells from freshly retrieved WT Xn. Cells were injected in 100μl 1:1 serum free medium/Matrigel (BD Biosciences, San Jose, CA).

Fluorescence-activated cell sorting (FACS) analysis

FACS analysis of fresh WT cells was performed as previously described (15). Small tumor pieces were dissociated into single cells, washed in RBCs lysis solution (comprised of: 8.3g NH_4Cl, 1.0g $KHCO_3$, 1.8ml of 5% EDTA in double distilled H_2O) at 1ml/5ml cell suspension ratio was applied for 2min in 4C◦. Cells were then filtered through a 30μm nylon mesh before final centrifugation.

Assessment of the percentage of NCAM1 surface marker:

All cells were re-suspended in FACS buffer consisting of 0.5% bovine serum albumin (BSA; Sigma-Aldrich, St. Louis) and 0.02% sodium azide in PBS. NCAM1 Surface antigen was labeled by incubation with fluorochrome conjugated antibody (eBioscience, San Diego, CA) at a concentration of 1µg antibody per 106 cells for 30min, in the dark, at 4°C to prevent internalization of antibodies. In addition, we used 7-amino-actinomycin-D (7AAD; eBioscience, San Diego, CA) for viable cell gating. All washing steps were performed in FACS buffer. All Quantitative measurements were made in comparison to IgG isotype antibody (eBioscience, San Diego, CA).

Assessment of the percentage of cells with high ALDH1 enzymatic activity

Detection of cells with high ALDH1 enzymatic activity was performed using the ALDEFLUOR kit (StemCell Technologies, Durham, NC, USA) as previously described (28, 29). Cells were suspended in Aldefluor assay buffer containing BODIPY-aminoacetaldehyde (BAAA), an uncharged ALDH1 substrate followed by incubation for 30-45 min at 37°C, in the dark. BAAA is taken up only by living cells through passive diffusion and then converted intracellular by ALDH1 into BODIPY-aminoacetate, a negatively charged reaction product, which is retained inside cells expressing high levels of ALDH1, resulting in these cells becoming brightly fluorescent. The fluorescent of these ALDH1 expressing cells (ALDH1+) can be detected by the green fluorescence channel (520-540 nm) of the FACSAria (BD Biosciences, San Jose, CA). As a negative control, for each sample of cells an aliquot treated in the same conditions was additionally incubated with diethylaminobenzaldehyde (DEAB), a specific ALDH1 inhibitor. Incubation of cells with the BAAA without the addition of DEAB resulted in a shift in BAAA fluorescence defining the ALDH1+ population. Since only cells with an intact cellular membrane could retain the Aldefluor reaction product, only viable ALDH1+ cells were identified.

FACS sorting

Cells were harvested as described above, filtered through a 30µm nylon mesh before final centrifugation, and then re-suspended in either in a FACS buffer or in an

ALDEFLUOR buffer. When WT Xn cells were sorted, possible contaminating mouse cells were eliminated from cells by discarding H2K+ (with an anti-H2Kd antibody - Miltenyi Biotech, Germany,). FACSAria was used in order to enrich for cells expressing surface markers and ALDH1 high activity. A 100-µm nozzle (BD Biosciences, San Jose, CA), sheath pressure of 20–25 pounds per square inch (PSI), and an acquisition rate of 1,000–3,000 events per second were used as conditions optimized for WT cell sorting. Single viable cells were gated on the basis of 7AAD, and then physically sorted into collection tubes for all subsequent experiments. Data was additionally analyzed and presented using FlowJo software.

Chip Array

The chip array data is deposited in publicly library (GEO); accession numbers GSE57269. All experiments were performed using Affymetrix HU GENE1.0st oligonucleotide arrays (Rivera and Haber, 2005). Total RNA from each sample was used to prepare biotinylated target DNA, according to the manufacturer's recommendations. The target cDNA generated from each sample was processed as per manufacturer's recommendation using an Affymetrix Gene Chip Instrument System. Details of quality control measures can be found online. Significantly changed genes were filtered as changed by at least twofold (p-value: 0.05). See also Supplemental Experimental Procedures.

Quantitative Real Time reverse transcription PCR analysis – Gene expression analysis

Quantitative reverse transcription PCR (qRT-PCR) was carried out to determine fold changes in expression of a selection of genes. Total RNA from cells was isolated using an RNeasy Micro Kit (Qiagen GmbH, Hilden, Germany) according to the manufacturer's instructions. cDNA was synthesized using a High Capacity cDNA Reverse Transcription kit (Applied Biosystems, California USA) on total RNA. Real-time PCR was performed using an ABI7900HT sequence detection system (Perkin-Elmer/Applied Biosystems, California, USA) in the presence of TaqMan Gene Expression Master Mix (Applied Biosystems, California, USA). PCR amplification was performed using gene specific TaqMan Gene Expression Assay-Pre-Made kits (Applied Biosystems, California, USA). Each analysis reaction was performed in

triplicate. HPRT1 or GAPDH were used as an endogenous control throughout the experimental analyses. PCR results were analyzed using SDS RQ Manager 1.2 software. Statistical analysis was performed using a non-paired 2-tails T-test. Statistical significance was considered at $P<0.05$.

Reverse phase protein array (RPPA)

Phosphorylated and unphosphorylated components of cell signaling pathways were quantified by RPPA as previously described (Tibes R, et al. Reverse phase protein array: validation of a novel proteomic technology and utility for analysis of primary leukemia specimens and hematopoietic stem cells. Mol Cancer Ther. 2006;5(10):2512–2521.). Briefly, protein extracts were prepared from un-sorted and ALDH1+ derived WT Xn. Following quantification, extracts were denatured and diluted in 5 serial 2-fold serial dilutions, which were then arrayed on multiple slides along with positive and negative controls prepared from mixed cell lysates or dilution buffer. Each slide was probed with a validated primary antibody and with a biotin-conjugated secondary antibody. After staining, slides were scanned, and spot intensities were analyzed, quantified, and normalized.

H&E staining

H&E staining of paraffin-embedded tissues: 5µm sections of paraffin-embedded tissues were mounted on super frost/plus glass and incubated at 60ºC for 40 minutes. After deparaffinization, slides were incubated in Mayer's Hematoxylin solution (Sigma-Aldrich) and incubated with 1% HCl in 70% ethanol for 1 minute. Slides were then incubated for 10 seconds in Eosin (Sigma-Aldrich). Images were produced using Olympus BX51TF.

Immunohistochemical staining of primary WT and WT Xn.

Sections, 4-µm thick, were cut from primary WT and WT Xn for immunohistochemistry. Immunostainings were performed as previously described (9). Brifly, the sections were processed within 1 week to avoid oxidation of antigens. Before immunostaining, sections were treated with 10mM citrate buffer, PH 6.0 for 10 min at 97ºC for antigen retrieval, followed by 3% H2O2 for 10 min. The slides were subsequently stained using the labeled strepavidin-biotin (LAB-SA) method using a Histostain plus kit (Zymed, San Francisco, CA, USA). Anti human NCAM

antibody (LifeSpan Biosciences, Inc. Seattle, WA, USA) was used at a dilution of 1:250. The immunoreaction was visualized by an HRP-based chromogen/substrate system (liquid DAB substrate kit – Zymed, San Francisco, CA, USA).

Western Blot

PWT, hFK and WT Xn cells were lysed in a buffer containing 50mM Tris-HCl, 150mM NaCl, 0.1mM EDTA, 0.5mM DTT, 1.5mM MgCl, 0.5% Triton-X. Total protein concentration was determined using the BCA protein assay kit (Thermo Scientific, Kalamazoo, MI). Proteins (100μg) were denatured in laemmli sample buffer (Bio-rad, Hercules, CA) (5 min, 950 C) and then separated on SDS-10% polyacrylamide gels. After electrophoresis, proteins were transferred to nitrocellulose membranes, which were then blocked overnight at 4°C, with 5% nonfat dry milk .Membranes were then incubated with anti-SIX2 (Affinity Bioreagents, Golden, CO, 1:200) / anti-E-Cadherin (Cell Signaling technology, #3195, 1:500) / anti VIMENTIN (abcam, #ab8978, 1:100) primary antibodies for 60 min and later with, goat anti-rabbit IgG secondary antibodies for 60 min. The membrane was reacted with ECL substrate (Thermo scientific) and then exposed to medical x-ray film (Fuji) for detection of antibody-bound protein bands.

IF staining of cells

Cells were fixed with 2% PFA with 3% sucrose in PBS (for SIX2 primary antibody) or with 4% PFA (for MNF and E-cadherin) for 10 min, and washed with PBS. Cells were blocked with 5% human serum, 5% donkey serum and 1% BSA in PBS–Tween (0.05%) followed by incubation a primary antibodies for SIX2 (Novus, cat# aa264-277), MNF (Dako, cat# M0821) or E-cadherin (Cell Signaling, cat#24E10) for 1 h in room temperature. Cells were washed and then incubated with a secondary antibody for 1 h in room temperature. Mounting containing DAPI (Dapi Fluoromount-G; SouthernBiotech, #0100-20) was applied. Images were obtained by Olympus BX51 fluorescence microscope using Olympus DP72 camera and cellSens standard software.